介子束流-核子反应中的强子单举产生及其动力学

刘 翔

xiangliu@lzu.edu.cn

兰州大学

2026年轻强子专题研讨会

2026年5月14日-18日 河南商丘

Outline

- The role of meson beam experiments in hadron spectroscopy research
- $\eta_1(1855)$ production by kaon induced reactions
- Production of hidden-strange molecular pentaquark
- Production of high-spin ω_J and ρ_J $(J = 2,3,4,5)$
- Summary

1. 介子束流实验在强子谱研究中的作用

第 42 卷 第 1 期
2025 年 3 月

原 子 核 物 理 评 论
Nuclear Physics Review

Vol. 42, No. 1
Mar., 2025

文章编号： 1007-4627(2025)01-0010-15

编辑推荐

国内外介子束流实验的发展现状和未来计划

王晓云[1], 刘 翔[2,3,4,5,6,†]

(1. 兰州理工大学理学院, 兰州 730050;
2. 兰州大学物理科学与技术学院, 兰州 730000;
3. 兰州理论物理中心, 兰州 730000;
4. 甘肃省理论物理重点实验室, 兰州 730000;
5. 量子理论与应用基础教育部重点实验室, 兰州 730000;
6. 教育部稀有同位素前沿科学中心, 兰州 730000)

摘要： 介子束流与原子核碰撞实验在中高能核物理和粒子物理研究领域发挥了重要推动作用，特别是在强子谱研究方面取得了一系列重要实验测量结果。本工作对目前国际上几个比较典型的介子束流实验进行了梳理与总结，这包括了位于日本的 J-PARC 实验、欧洲核子中心的 COMPASS 实验、AMBER 实验以及计划中的 HIKE 实验、美国 JLab 的 GlueX 实验和 EIC 项目。进一步，基于国内的 HIAF 装置对可能产生的次级介子束流的参数指标进行了分析估算，并讨论了可以开展地相关物理测量。通过对这些实验项目的调研分析，旨在为进一步规划和建造我国的介子束流实验装置并开展强子物理方面的研究有所启发和借鉴。

关键词： 介子束流实验；强子物理；中高能核物理
中图分类号： O571.53　　**文献标志码：** A
DOI： 10.11804/NuclPhysRev.42.2024008　　**CSTR：** 32260.14.NuclPhysRev.42.2024008

1. 介子束流实验在强子谱研究中的作用

表 1　PDG 中收录的轻介子谱[5](勾选的粒子都被介子束流实验进行过测量)

粒子	J^P	介子束流实验	粒子	J^P	介子束流实验	粒子	J^P	介子束流实验	粒子	J^P	介子束流实验
η	0^-	√	$\rho(1450)$	1^-		$\eta_2(1870)$	2^-	√	$\rho_5(2350)$	5^-	√
$f_0(500)$	0^+		$\eta(1475)$	0^-	√	$\pi_2(1880)$	2^-	√	$f_6(2510)$	6^+	√
$\rho(770)$	1^-	√	$f_0(1500)$	0^+	√	$\rho(1900)$	1^-		$K_0^*(700)$	0^+	√
$\omega(782)$	1^-	√	$f_1(1510)$	1^+	√	$f_2(1910)$	2^+	√	$K^*(892)$	1^-	√
$\eta'(958)$	0^-	√	$f_2'(1525)$	2^+	√	$a_0(1950)$	0^+		$K_1(1270)$	1^+	√
$f_0(980)$	0^+	√	$f_2(1565)$	2^+	√	$f_2(1950)$	2^+	√	$K_1(1400)$	1^+	√
$a_0(980)$	0^+	√	$\rho(1570)$	1^-	√	$\rho_3(1990)$	3^-		$K^*(1410)$	1^-	√
$\phi(1020)$	1^-	√	$h_1(1595)$	1^+	√	$\pi_2(2005)$	2^-	√	$K_0^*(1430)$	0^+	√
$h_1(1170)$	1^+	√	$\pi_1(1600)$	1^-	√	$f_2(2010)$	2^+	√	$K_2^*(1430)$	2^+	√
$b_1(1235)$	1^+	√	$a_1(1640)$	1^+	√	$f_0(2020)$	0^+	√	$K(1460)$	0^-	√
$a_1(1260)$	1^+	√	$f_2(1640)$	2^+	√	$a_4(2040)$	4^+	√	$K_2(1580)$	2^-	√
$f_2(1270)$	2^+	√	$\eta_2(1645)$	2^-		$f_4(2050)$	4^+	√	$K(1630)$	?	√
$f_1(1285)$	1^+	√	$\omega(1650)$	1^-		$\pi_2(2100)$	2^-	√	$K_1(1650)$	1^+	√
$\eta(1295)$	0^-		$\omega_3(1670)$	3^-	√	$f_0(2100)$	0^+		$K^*(1680)$	1^-	√
$\pi(1300)$	0^-		$\pi_2(1670)$	2^-	√	$f_2(2150)$	2^+		$K_2(1770)$	2^-	√
$a_2(1320)$	2^+	√	$\phi(1680)$	1^-		$\rho(2150)$	1^-		$K_3^*(1780)$	3^-	√
$f_0(1370)$	0^+		$\rho_3(1690)$	3^-	√	$\phi(2170)$	1^-		$K_2(1820)$	2^-	√
$h_1(1380)$	1^+		$\rho(1700)$	1^-	√	$f_0(2200)$	0^+	√	$K(1830)$	0^-	√
$\pi_1(1400)$	1^-	√	$a_2(1700)$	2^+	√	$f_J(2220)$	$2^+,4^+$		$K_0^*(1950)$	0^+	√
$\eta(1405)$	0^-	√	$f_0(1710)$	0^+	√	$\eta(2225)$	0^-		$K_2^*(1980)$	2^+	√
$f_1(1420)$	1^+	√	$\eta(1760)$	0^-		$\rho_3(2250)$	3^-	√	$K_4^*(2045)$	4^+	√
$\omega(1420)$	1^-		$\pi(1800)$	0^-	√	$f_2(2300)$	2^+	√	$K_2(2250)$	2^-	√
$a_1(1420)$	1^+	√	$f_2(1810)$	2^+	√	$f_4(2300)$	4^+		$K_3(2320)$	3^+	√
$f_2(1430)$	2^+	√	$X(1835)$	0^-		$f_0(2330)$	0^+		$K_5^*(2380)$	5^-	√
$a_0(1450)$	0^+	√	$\pi_3(1850)$	3^-	√	$f_2(2340)$	2^+	√	$K_4(2500)$	4^-	√

PDG所收录的轻强子谱中的八成以上粒子及其相关谱学性质都来自介子束流与原子核碰撞实验

1. 介子束流实验在强子谱研究中的作用

当下对介子束流实验的布局仍然在不断推进

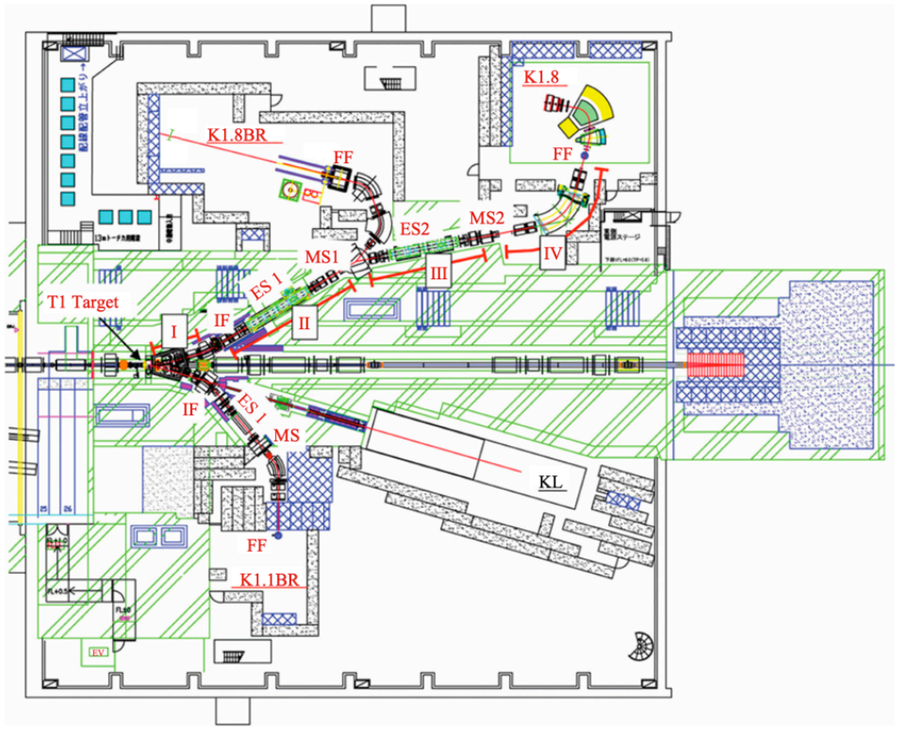

图 1　(在线彩图) J-PARC 的强子实验大厅、带电次级束流线 (K1.8、K1.8BR 和 K1.1BR) 以及各个实验区域的布局图[32]

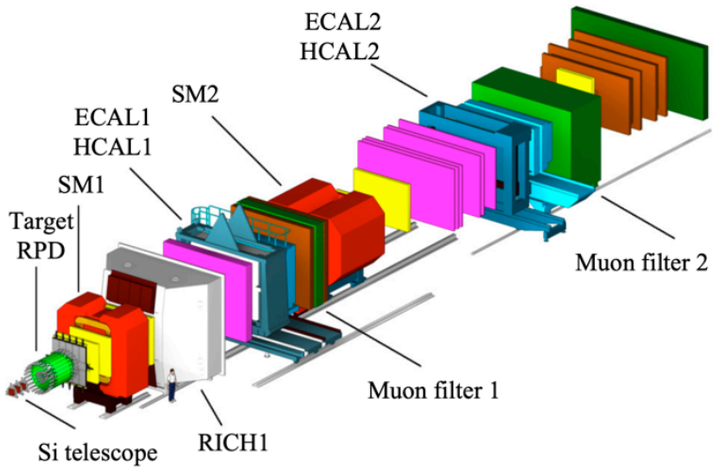

图 3　(在线彩图) 用于强子束测量的 COMPASS 装置三维视图

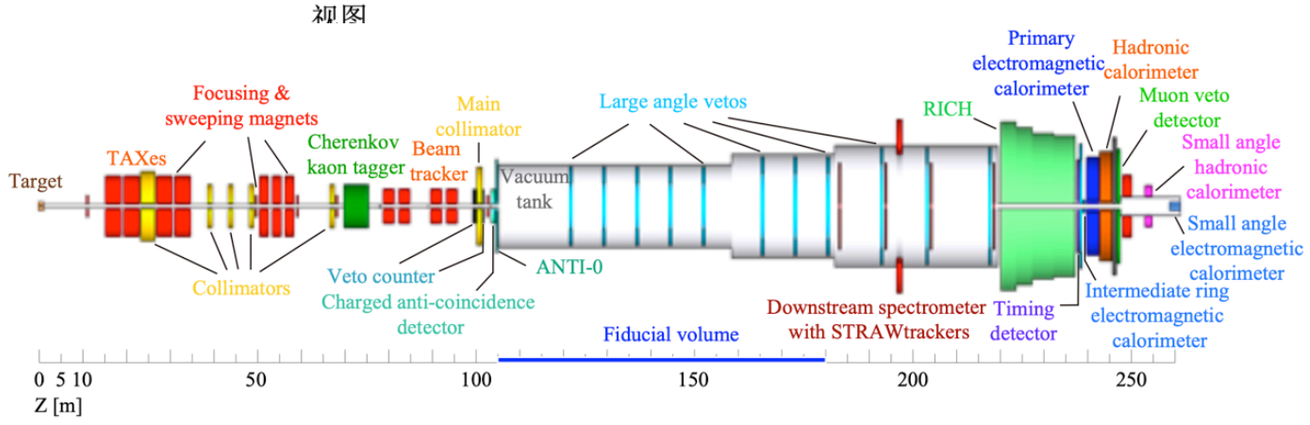

图 5　(在线彩图) HIKE 第一阶段的布局图[71](纵横比为 1∶10)

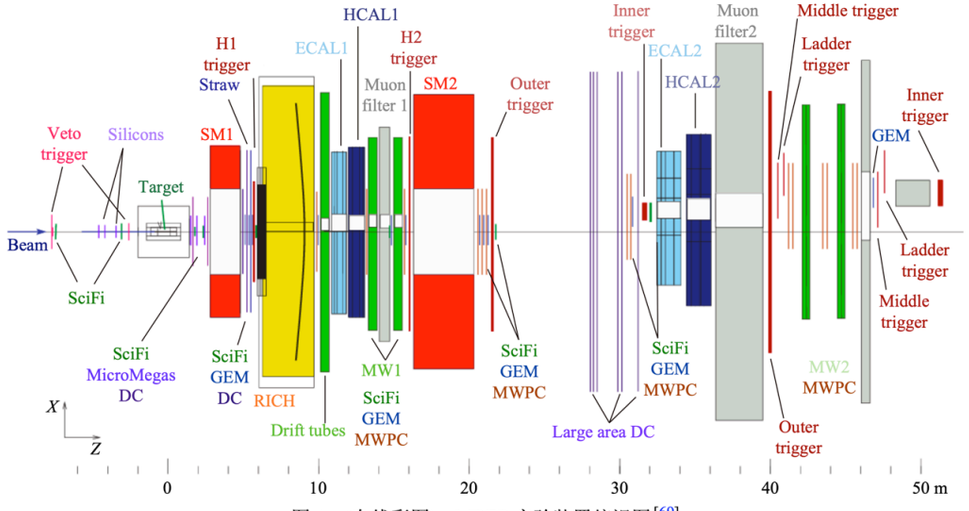

图 4　(在线彩图) AMBER 实验装置俯视图[69]

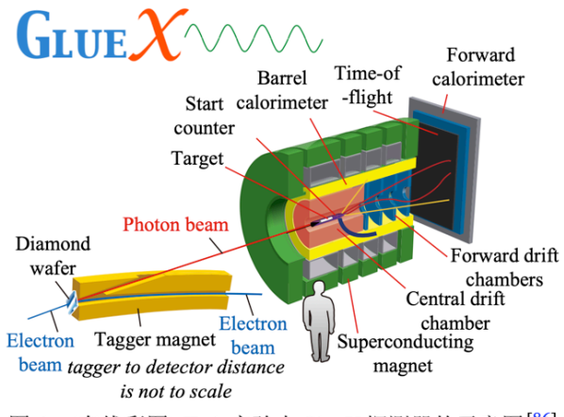

图 6　(在线彩图) JLab 实验中 GlueX 探测器的示意图[86]

2. $\eta_1(1855)$ production by kaon induced reactions

PHYSICAL REVIEW LETTERS **129,** 192002 (2022)

Observation of an Isoscalar Resonance with Exotic $J^{PC} = 1^{-+}$ Quantum Numbers in $J/\psi \to \gamma\eta\eta'$

Using a sample of $(10.09 \pm 0.04) \times 10^9$ J/ψ events collected with the BESIII detector operating at the BEPCII storage ring, a partial wave analysis of the decay $J/\psi \to \gamma\eta\eta'$ is performed. The first observation of an isoscalar state with exotic quantum numbers $J^{PC} = 1^{-+}$, denoted as $\eta_1(1855)$, is reported in the process $J/\psi \to \gamma\eta_1(1855)$ with $\eta_1(1855) \to \eta\eta'$. Its mass and width are measured to be $(1855 \pm 9^{+6}_{-1})$ MeV/c^2 and $(188 \pm 18^{+3}_{-8})$ MeV, respectively, where the first uncertainties are statistical and the second are systematic, and its statistical significance is estimated to be larger than 19σ.

TABLE I. The masses, widths, $\mathcal{B}(J/\psi \to \gamma X \to \gamma\eta\eta')$ or $\mathcal{B}(J/\psi \to \eta' h_1 \to \gamma\eta\eta')$ (B.F.), and statistical significances (Sig.) for each component in the baseline set of amplitudes. The first uncertainties are statistical, and the second are systematic.

Resonance	M (MeV/c^2)	Γ (MeV)	B.F.($\times 10^{-5}$)	Sig.
$f_0(1500)$	1506	112	$1.81 \pm 0.11^{+0.19}_{-0.13}$	$> 30\sigma$
$f_0(1810)$	1795	95	$0.11 \pm 0.01^{+0.04}_{-0.03}$	11.1σ
$f_0(2020)$	$2010 \pm 6^{+6}_{-4}$	$203 \pm 9^{+13}_{-11}$	$2.28 \pm 0.12^{+0.29}_{-0.20}$	24.6σ
$f_0(2330)$	$2312 \pm 7^{+7}_{-3}$	$65 \pm 10^{+3}_{-12}$	$0.10 \pm 0.02^{+0.01}_{-0.02}$	13.2σ
$\eta_1(1855)$	$1855 \pm 9^{+6}_{-1}$	$188 \pm 18^{+3}_{-8}$	$0.27 \pm 0.04^{+0.02}_{-0.04}$	21.4σ
$f_2(1565)$	1542	122	$0.32 \pm 0.05^{+0.12}_{-0.02}$	8.7σ
$f_2(2010)$	$2062 \pm 6^{+10}_{-7}$	$165 \pm 17^{+10}_{-5}$	$0.71 \pm 0.06^{+0.10}_{-0.06}$	13.4σ
$f_4(2050)$	2018	237	$0.06 \pm 0.01^{+0.03}_{-0.01}$	4.6σ
0^{++} PHSP	...	...	$1.44 \pm 0.15^{+0.10}_{-0.20}$	15.7σ
$h_1(1415)$	1416	90	$0.08 \pm 0.01^{+0.01}_{-0.02}$	10.2σ
$h_1(1595)$	1584	384	$0.16 \pm 0.02^{+0.03}_{-0.01}$	9.9σ

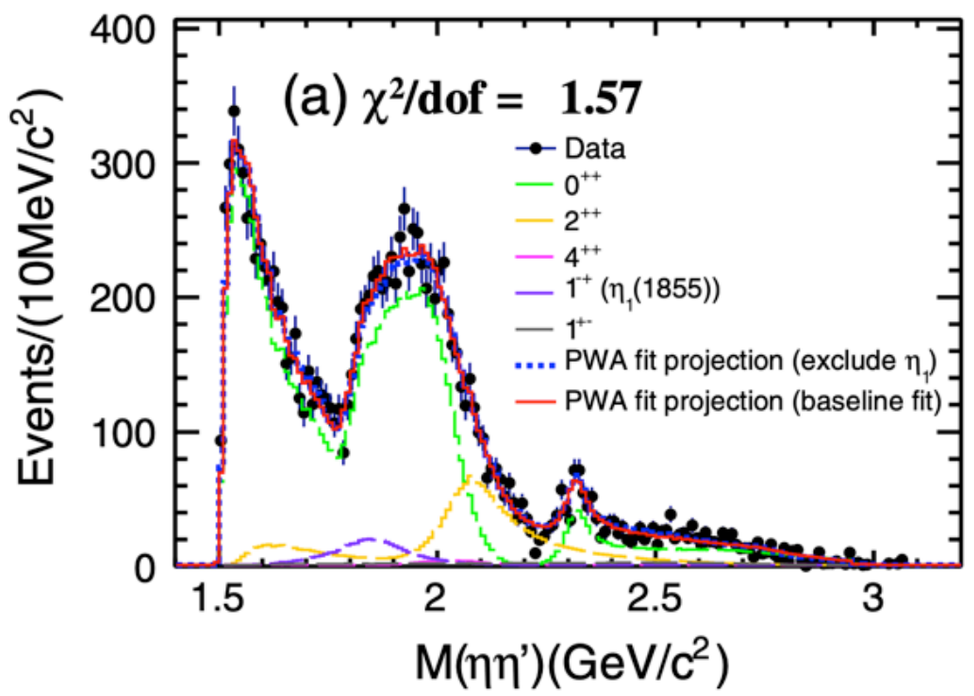

2. $\eta_1(1855)$ production by kaon induced reactions

PHYSICAL REVIEW D **108,** 054034 (2023)

Hybrid

Constructing the $J^{P(C)} = 1^{-(+)}$ light flavor hybrid nonet with the newly observed $\eta_1(1855)$

Bing Chen,[1,3,*] Si-Qiang Luo,[2,3,4,6,†] and Xiang Liu[2,3,4,5,6,‡]

The recently discovered $\eta_1(1855)$ and the previously observed $\pi_1(1600)$ state present a valuable opportunity for the investigation of the $J^{P(C)} = 1^{-(+)}$ light hybrid nonet. In this study, we employ a semirelativistic quark potential model to examine the masses of the $J^{P(C)} = 1^{-(+)}$ light hybrid states. The static potential, which portrays the confinement force between the quark-antiquark pair in a hybrid system, is borrowed from the SU(3) lattice gauge theory. Additionally, we utilize a constituent gluon model to analyze the strong decay characteristics of these light 1^{-+} hybrids. Our findings suggest that the $\pi_1(1600)$ and $\eta_1(1855)$ states could be potential candidates for 1^{-+} $(u\bar{u} - d\bar{d})g/\sqrt{2}$ and $s\bar{s}g$ hybrids, respectively. To ensure comprehensiveness, we also investigate the isospin partners of the $\pi_1(1600)$ and $\eta_1(1855)$ states within the $1^{-(+)}$ nonet—specifically, the $(u\bar{u} + d\bar{d})g/\sqrt{2}$ and $s\bar{q}g$ ($q = u$ and d quarks) states. We propose some potential decay channels which could be explored in experimental settings to detect these undiscovered states.

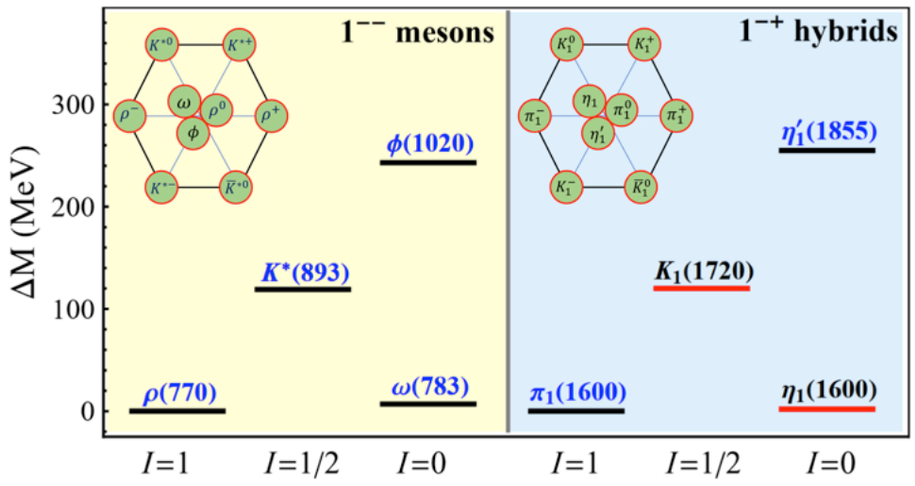

TABLE VI. The partial and total widths of the strong decays of the $\eta_1'(1^{-+})$ state (MeV).

$\eta\eta'$	K^*K	$K_1(1270)K$	Total	Exp. [40,41]
≈ 0	2	157	159	$188 \pm 18^{+3}_{-8}$

2. $\eta_1(1855)$ production by kaon induced reactions

SCIENCE CHINA
Physics, Mechanics & Astronomy

• Article •

June 2022 Vol. 65 No. 6: 261011
https://doi.org/10.1007/s11433-022-1887-5

Molecule

Interpretation of the $\eta_1(1855)$ as a $K\bar{K}_1(1400)$ + c.c. molecule

Xiang-Kun Dong[1,2], Yong-Hui Lin[3], and Bing-Song Zou[1,2,4*]

[1] *CAS Key Laboratory of Theoretical Physics, Institute of Theoretical Physics, Chinese Academy of Sciences, Beijing 100190, China;*
[2] *School of Physical Sciences, University of Chinese Academy of Sciences, Beijing 100049, China;*
[3] *Helmholtz-Institut für Strahlen-und Kernphysik and Bethe Center for Theoretical Physics, Universität Bonn, Bonn D-53115, Germany;*
[4] *School of Physics, Central South University, Changsha 410083, China*

Received February 3, 2022; accepted March 7, 2022; published online May 5, 2022

An exotic state with $J^{PC} = 1^{-+}$, denoted by $\eta_1(1855)$, was observed by BESIII Collaboration recently in $J/\psi \to \gamma\eta\eta'$. The fact that its mass is just below the threshold of $K\bar{K}_1(1400)$ stimulates us to investigate whether this exotic state can be interpreted as a $K\bar{K}_1(1400)$ + c.c. molecule or not. Using the one boson exchange model, we show that it is possible for $K\bar{K}_1(1400)$ with $J^{PC} = 1^{-+}$ to bind together by taking the momentum cutoff $\Lambda \gtrsim 2$ GeV and yield the same binding energy as the experimental value when $\Lambda \approx 2.5$ GeV. In this molecular picture, the predicted branch ratio $\mathrm{Br}(\eta_1(1855) \to \eta\eta') \approx 15\%$ is consistent with the experimental results, which again supports the molecular explanation of $\eta_1(1855)$. Relevant systems, namely $K\bar{K}_1(1400)$ with $J^{PC} = 1^{--}$ and $K\bar{K}_1(1270)$ with $J^{PC} = 1^{-\pm}$, are also investigated, some of which can be searched for in the future experiments.

Table 1 Partial widths of the isoscalar $K\bar{K}_1(1400)$ molecular states with quantum numbers 1^{--} and 1^{-+} with $\Lambda_0 = 1.3$ GeV and $\Lambda_1 = 2.5$ GeV. All the decay widths are in unit of MeV. Here, we assume 5% D-wave contribution in the $K_1K^*\pi$ and $K_1K^*\eta$ vertex

Mode	Widths (MeV)	
	1^{--} $E_B = 20$ MeV	1^{-+} $E_B = 40$ MeV
$K^*\bar{K}^*$	38.1	26.3
$K\bar{K}$	0.5	0
$K\bar{K}^*$	1.0	0.9
$a_1\pi$	0	9.2
$f_1\eta$	0	0.2
$\eta\eta'$	0	26.9
$\sigma\omega$	0.2	0
$\rho\rho$	0	0.04
$\pi\rho$	6.4	0
$\eta\omega$	0.4	0
$\omega\omega$	0	0.01
$\omega\phi$	0	0.4
$K\bar{K}^*\pi$	130.0	105.0
2-body	46.5	64.0
Total	176.5	169.0

2. $\eta_1(1855)$ production by kaon induced reactions

Kaon induced reactions can be applied to distinguish two hadronic configurations

PHYSICAL REVIEW D **106,** 036005 (2022)

Production of the $\eta_1(1855)$ through kaon induced reactions under the assumptions that it is a molecular or a hybrid state

Xiao-Yun Wang,[1,2,*] Fan-Cong Zeng,[3] and Xiang Liu[4,5,2,6,7,†]

[1]*Department of physics, Lanzhou University of Technology, Lanzhou 730050, China*
[2]*Lanzhou Center for Theoretical Physics, Key Laboratory of Theoretical Physics of Gansu Province, Lanzhou University, Lanzhou, Gansu 730000, China*
[3]*University of Chinese Academy of Sciences, Beijing 100049, China*
[4]*School of Physical Science and Technology, Lanzhou University, Lanzhou 730000, China*
[5]*Research Center for Hadron and CSR Physics, Lanzhou University and Institute of Modern Physics of CAS, Lanzhou 730000, China*
[6]*Frontiers Science Center for Rare Isotopes, Lanzhou University, Lanzhou 730000, China*
[7]*Joint Research Center for Physics, Lanzhou University and Qinghai Normal University, Xining 810000, China*

(Received 21 May 2022; accepted 27 July 2022; published 4 August 2022)

By the reaction of kaon interacting with a proton, we investigate the production of the newly observed $\eta_1(1855)$ predicted in the picture of the $K\bar{K}_1(1400)$ molecular state and hybrid state. The total and differential cross sections of the concrete $K^- p \to \eta_1(1855)\Lambda$ reaction are calculated. Taking the partial decay width of the η_1 to $K\bar{K}^*$ as 0.9 MeV and 98.1 MeV, the minimum cross section of the $\eta_1(1855)$ production via the $K^- p$ reaction can reach up 0.59 nb and 63.8 nb at the center of mass energies $W \simeq 3.5$ GeV, respectively. The differential cross sections for the $\eta_1(1855)$ production at the different center of mass energies are also available. Furthermore, we present the Dalitz processes of $2 \to 3$ and $2 \to 4$, and initially discuss the feasibility of finding out the $\eta_1(1855)$ in experiments like J-PARC.

2. $\eta_1(1855)$ production by kaon induced reactions

Different decay behaviors for two scenarios

TABLE I. The calculated partial decay widths (in units of MeV) of the $\eta_1(1855)$ under the hybrid [4] and molecular [7] pictures.

	$\eta_1(1855)$ $(J^{PC}=1^{-+})$	
Channel	Hybrid state [4]	Molecule state [7]
$K^*\bar{K}^*$	...	26.3
$K\bar{K}$	...	0
$K\bar{K}^*$	98.1	0.9
$a_1\pi$	...	9.2
$f_1\eta$	...	0.2
$\eta\eta'$	0.7–1.8	26.9
$\sigma\omega$	...	0
$\rho\rho$	...	0.04
$\pi\rho$	...	0
$\eta\omega$	...	0
$\omega\omega$	...	0.01
$\omega\phi$	...	0.4
$K_1(1270)\bar{K}$	30.4	...
$K\bar{K}^*\pi$	...	105.0

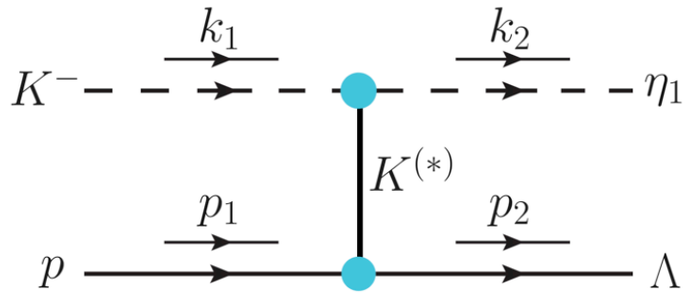

FIG. 1. Schematic diagram for the t-channel contribution to the $K^- p \to \eta_1(1855)\Lambda$ reaction.

$$\mathcal{L}_{\eta_1 KK} = -ig_{\eta_1 KK}[(\partial^\mu K)\bar{K} - (\partial^\mu \bar{K})K]\eta_{1\mu},$$

$$\mathcal{L}_{KN\Lambda} = ig_{KN\Lambda}\bar{N}\gamma_5\Lambda K + \text{H.c.},$$

$$\mathcal{L}_{\eta_1 K^* K} = \frac{g_{\eta_1 K^* K}}{m_{\eta_1}}\epsilon_{\alpha\beta\mu\nu}\partial^\beta \eta_1^\alpha \partial^\nu K^{*\mu} K,$$

$$\mathcal{L}_{K^* N\Lambda} = -g_{K^* N\Lambda}\bar{N}\left(\not{K}^* - \frac{\kappa_{K^* N\Lambda}}{2m_N}\sigma_{\mu\nu}\partial^\nu K^{*\mu}\right)\Lambda + \text{H.c.},$$

2. $\eta_1(1855)$ production by kaon induced reactions

Different decay behaviors for two scenarios

TABLE I. The calculated partial decay widths (in units of MeV) of the $\eta_1(1855)$ under the hybrid [4] and molecular [7] pictures.

	$\eta_1(1855)$ $(J^{PC}=1^{-+})$	
Channel	Hybrid state [4]	Molecule state [7]
$K^*\bar{K}^*$	...	26.3
$K\bar{K}$	...	0
$K\bar{K}^*$	98.1	0.9
$a_1\pi$	...	9.2
$f_1\eta$	...	0.2
$\eta\eta'$	0.7–1.8	26.9
$\sigma\omega$	...	0
$\rho\rho$	...	0.04
$\pi\rho$	...	0
$\eta\omega$	...	0
$\omega\omega$	...	0.01
$\omega\phi$	...	0.4
$K_1(1270)\bar{K}$	30.4	...
$K\bar{K}^*\pi$	...	105.0

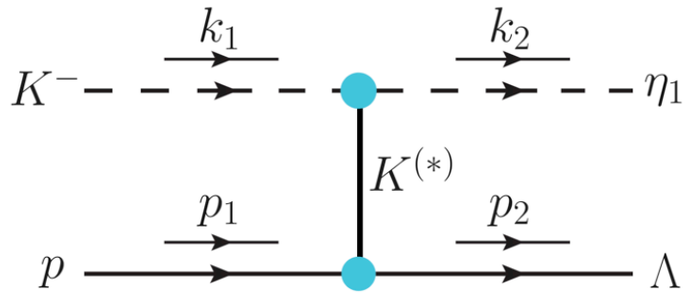

FIG. 1. Schematic diagram for the t-channel contribution to the $K^-p \to \eta_1(1855)\Lambda$ reaction.

With the above Lagrangians, the amplitude of the $\eta_1(1855)$ production via t-channel K^* exchange in the K^-p scatterings can be written as

$$i\mathcal{M}_{K^*} = i\frac{g_{\eta_1 K^* K}}{m_{\eta_1}} g_{K^* N\Lambda} F(q^2)\bar{u}_N(p_2)\left(\gamma_\nu - \frac{\kappa_{K^* N\Lambda}}{2m_N}\gamma_\nu \not{q}_{K^*}\right) \times \epsilon_{\alpha\beta\mu\xi}\frac{\mathcal{P}^{\mu\nu}}{t-m_{K^*}^2} k_2^\beta \epsilon_{\eta_1}^\alpha (k_1-k_2)^\xi \quad (6)$$

with

$$\mathcal{P}^{\mu\nu} = -i(g^{\mu\nu} + q_{K^*}^\mu q_{K^*}^\nu / m_{K^*}^2), \quad (7)$$

2. $\eta_1(1855)$ production by kaon induced reactions

Production rates are different

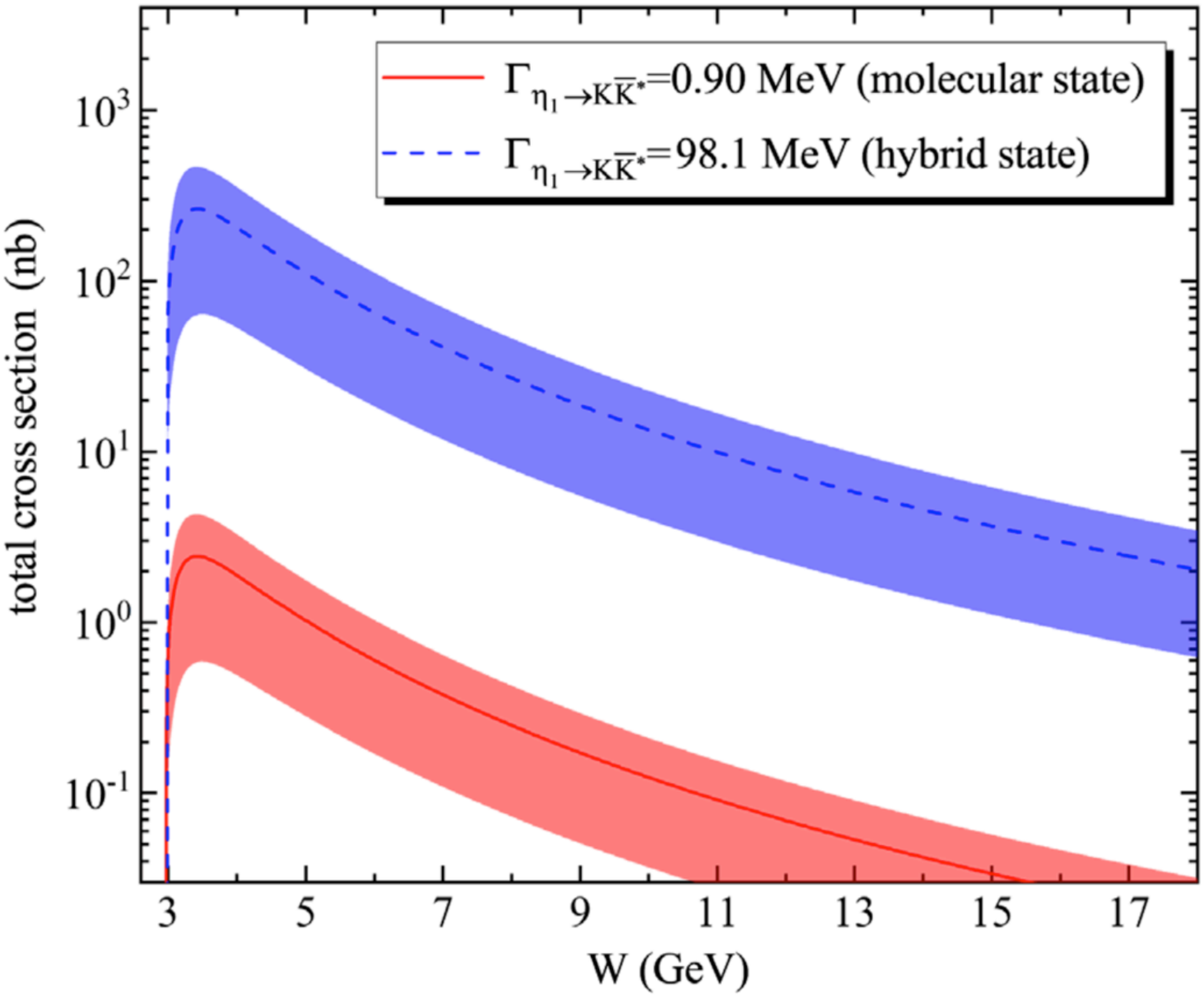

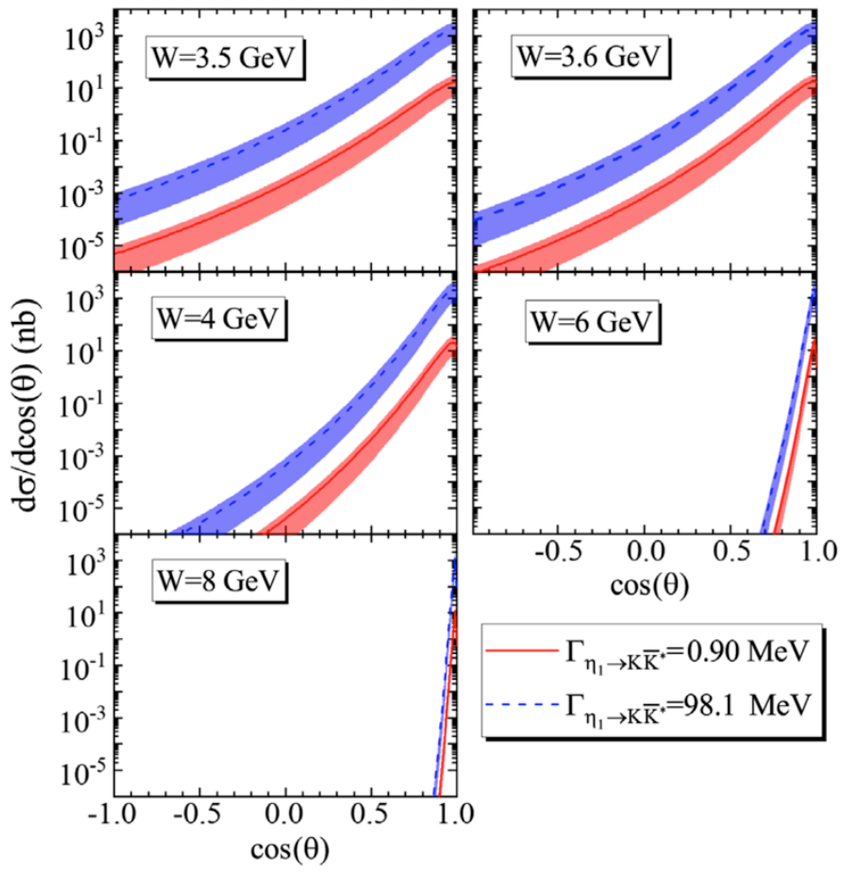

FIG. 3. The differential cross section $d\sigma/d\cos\theta$ of the $\eta_1(1855)$ production at different c.m. energies $W = 3.5$ GeV, 3.6 GeV, 4, 6 GeV and 8 GeV. Here, the notation is the same as that in Fig. 2.

3. Production of hidden-strange molecular pentaquark

$N^*(2080)$ has been proposed as a $K^*\Sigma$ molecular state, potentially serving as the strange partner of the $P_c(4457)$

Citation: S. Navas *et al.* (Particle Data Group), Phys. Rev. D **110**, 030001 (2024) and 2025 update

$N(1875)$ $3/2^-$ $I(J^P) = \frac{1}{2}(\frac{3}{2}^-)$ Status: ***

was $N(2080)$

Before the 2012 *Review*, all the evidence for a $J^P = 3/2^-$ state with a mass above 1800 MeV was filed under a two-star $N(2080)$. There is now evidence from ANISOVICH 12A for two $3/2^-$ states in this region, so we have split the older data (according to mass) between a three-star $N(1875)$ and a two-star $N(2120)$.

$N(1875)$ POLE POSITION

REAL PART

VALUE (MeV)	*DOCUMENT ID*	*TECN*	*COMMENT*
1850 to 1950 (≈ 1900) OUR ESTIMATE			

Citation: S. Navas *et al.* (Particle Data Group), Phys. Rev. D **110**, 030001 (2024) and 2025 update

$N(2120)$ $3/2^-$ $I(J^P) = \frac{1}{2}(\frac{3}{2}^-)$ Status: ***

Before the 2012 *Review*, all the evidence for a $J^P = 3/2^-$ state with a mass above 1800 MeV was filed under a two-star $N(2080)$. There is now evidence from ANISOVICH 12A for two $3/2^-$ states in this region, so we have split the older data (according to mass) between a three-star $N(1875)$ and a two-star $N(2120)$.

$N(2120)$ POLE POSITION

REAL PART

VALUE (MeV)	*DOCUMENT ID*	*TECN*	*COMMENT*
2050 to 2150 (≈ 2100) OUR ESTIMATE			

$$J^P = 1/2^+ : P_{s\bar{s}}[1/2^-]$$

$$J^P = 3/2^+ : P_{s\bar{s}}[3/2^-]$$

J. He, Nucleon resonances $N(1875)$ and $N(2100)$ as strange partners of LHCb pentaquarks, Phys. Rev. D **95**, 074031 (2017).

Y. H. Lin, C. W. Shen, and B. S. Zou, Decay behavior of the strange and beauty partners of P_c hadronic molecules, Nucl. Phys. **A980**, 21 (2018).

K. P. Khemchandani, H. Kaneko, H. Nagahiro, and A. Hosaka, Vector meson-Baryon dynamics and generation of resonances, Phys. Rev. D **83**, 114041 (2011).

M. Doring, E. Oset, and B. S. Zou, The role of the $N^*(1535)$ resonance and the $\pi^- p \to KY$ amplitudes in the OZI forbidden $\pi N \to \phi N$ reaction, Phys. Rev. C **78**, 025207 (2008).

3. Production of hidden-strange molecular pentaquark

PHYSICAL REVIEW D **111,** 034021 (2025)

Production potential of hidden-strange molecular pentaquarks through the $\pi^- p \to K^* \Sigma$ process

Xiao-Yun Wang,[1,2,*] Yuan Gao,[1] and Xiang Liu[2,3,4,5,6,†]

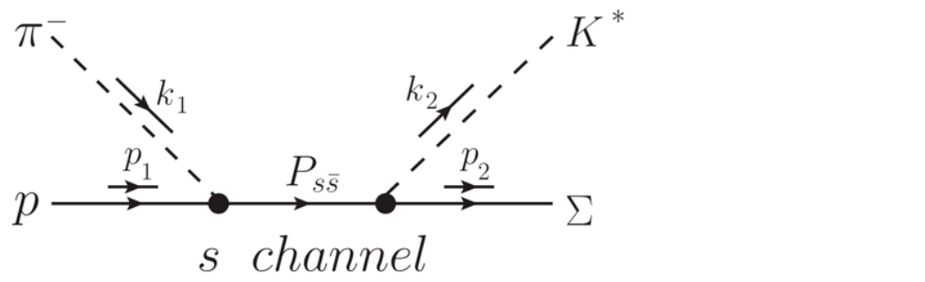

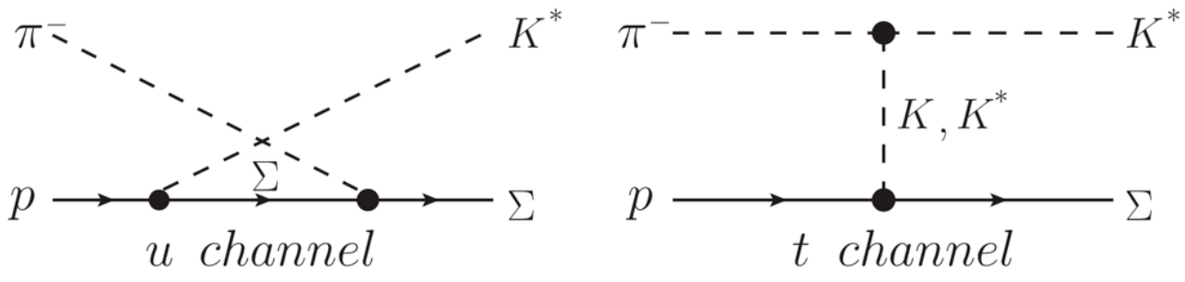

FIG. 1. Feynman diagrams for the $\pi^- p \to K^* \Sigma$ reaction.

Based on the above Lagrangians, the scattering amplitude for the reaction $\pi^- p \to K^* \Sigma$ is given by

$$\mathcal{M} = \epsilon^{\mu}(k_2)\bar{u}(p_2)(\mathcal{A}_{s,\mu} + \mathcal{A}_{u,\mu} + \mathcal{A}_{t,\mu})u(p_1), \tag{18}$$

where ϵ^{μ} denotes the polarization vector of the outgoing K^* meson, while $\bar{u}$ and u represent the Dirac spinors for the outgoing Σ baryon and the incoming proton, respectively.

The reduced amplitudes $\mathcal{A}_{s,\mu}$, $\mathcal{A}_{u,\mu}$, and $\mathcal{A}_{t,\mu}$ for the s-, u-, and t-channel contributions read as

$$\mathcal{A}_{s,\mu}^{P^*(3/2^-)} = \sqrt{2} g_{K^*\Sigma P^*}^{3/2^-} \frac{g_{\pi N P^*}^{3/2^-}}{m_\pi} F_s(q)\gamma_5 k_1^{\nu} \times \frac{(\not{q}_s + m_{P^*})}{s - m_{P^*}^2 + i m_{P^*}\Gamma_{P^*}} \Delta_{\mu\nu}, \tag{19}$$

$$\mathcal{A}_{s,\mu}^{P^*(1/2^-)} = -i\sqrt{2} g_{K^*\Sigma P^*}^{1/2^-} g_{\pi N P^*}^{1/2^-} F_s(q)\gamma_5\gamma_\mu \times \frac{(\not{q}_s + m_{P^*})}{s - m_{P^*}^2 + i m_{P^*}\Gamma_{P^*}}, \tag{20}$$

$$\mathcal{A}_{u,\mu}^{\Sigma} = -i\sqrt{2}\frac{g_{\Sigma\Sigma\pi}}{m_\pi} g_{K^*N\Sigma} F_u(q)\gamma^5\gamma^{\nu} k_{1\nu} \frac{(\not{q}_\Sigma + m_\Sigma)}{u - m_\Sigma^2} \times \left(\gamma_\mu - \frac{k_{K^*\Sigma N}}{2m_N}\gamma_\mu \not{q}_{K^*}\right), \tag{21}$$

$$\mathcal{A}_{t,\mu}^{K} = i\sqrt{2} g_{K^*K\pi} g_{K\Sigma N} F_t(q) \frac{1}{t - m_K^2}\gamma_5 \times [k_{1\mu} + (k_1 - k_2)_\mu], \tag{22}$$

$$\mathcal{A}_{t,\mu}^{K^*} = i\sqrt{2} g_{\pi K^* K^*} g_{K^*N\Sigma} F_t(q)\left(\gamma_\xi - \frac{k_{K^*\Sigma N}}{2m_N}\gamma_\xi \not{q}_{K^*}\right) \times \epsilon_{\mu\nu\alpha\beta}\frac{\mathcal{P}^{\nu\xi}}{t - m_{K^*}^2} k_2^{\alpha}(k_1 - k_2)^{\beta} \tag{23}$$

3. Production of hidden-strange molecular pentaquark

$$J^P = 3/2^+ : P_{s\bar{s}}[3/2^-]$$

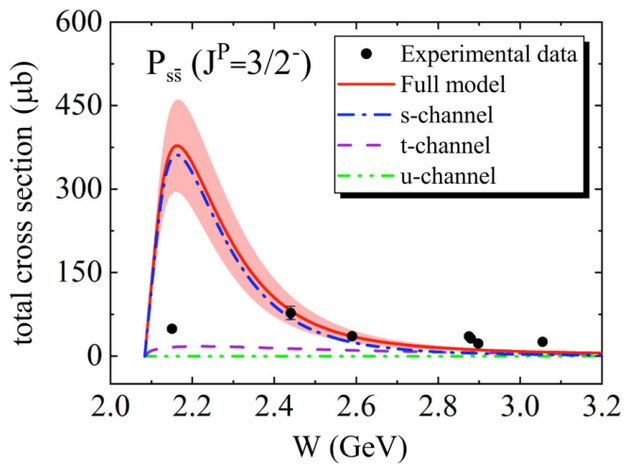

FIG. 2. The total cross section for the reaction $\pi^- p \to K^*\Sigma$. The band stands for the error bar of the five fitting parameters in Table I. The solid (red), dashed-dotted (blue), dashed (purple), dash–double dotted (green) lines are for the full model, the s-channel, the t-channel and the u-channel, respectively. Here, the spin-parity quantum number of the $P_{s\bar{s}}$ is $\frac{3}{2}^-$.

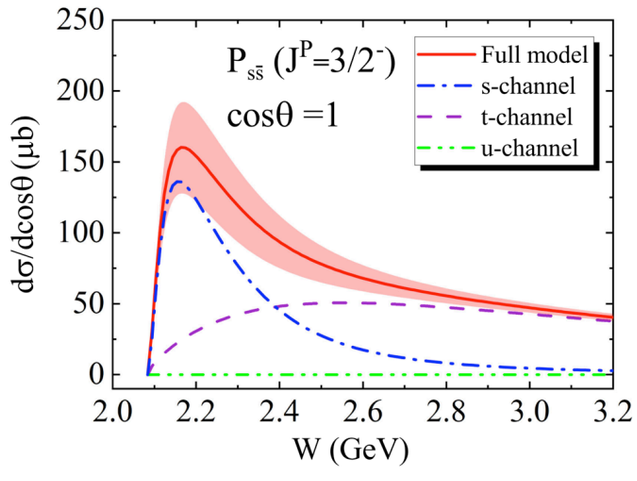

FIG. 4. The differential cross-section $d\sigma/d\cos\theta$ for the $\pi^- p \to K^*\Sigma$ reaction varies with different c.m. energies when $\cos\theta = 1$. Here, the notation is the same as that in Fig. 2.

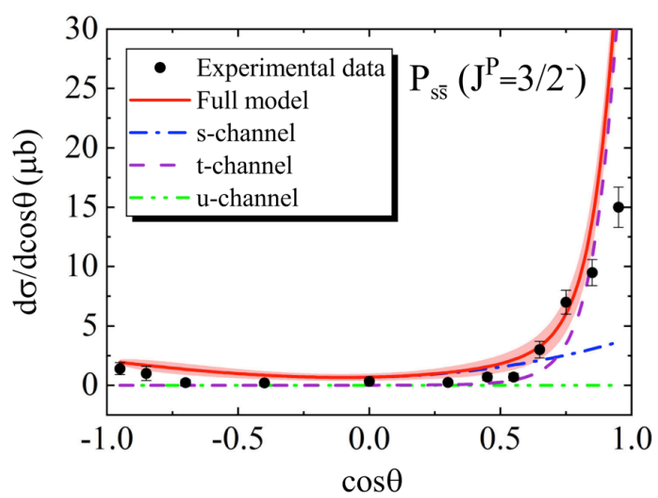

FIG. 3. The differential cross-section $d\sigma/d\cos\theta$ for the $\pi^- p \to K^*\Sigma$ reaction as a function of $\cos\theta$. The experimental data are from Ref. [35]. Here, the notation is the same as that in Fig. 2.

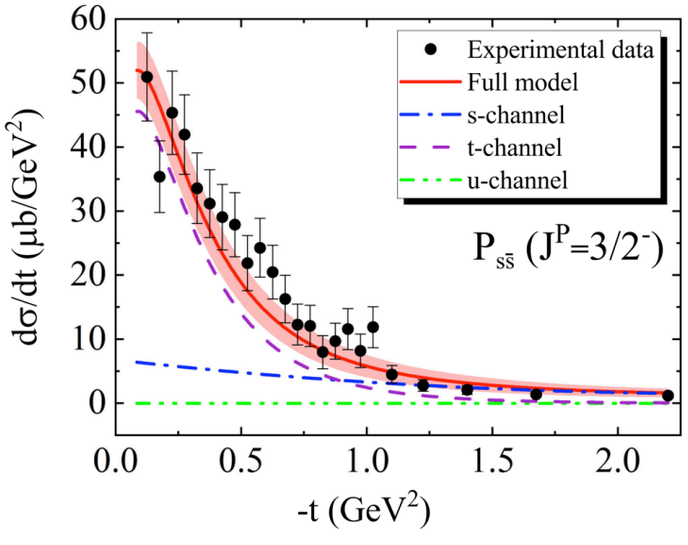

FIG. 6. The t distribution for the reaction $\pi^- p \to K^*\Sigma$. The experimental data are from Ref. [36]. Here, the notation is the same as that in Fig. 2.

3. Production of hidden-strange molecular pentaquark

$$J^P = 1/2^+ : P_{s\bar{s}}[1/2^-]$$

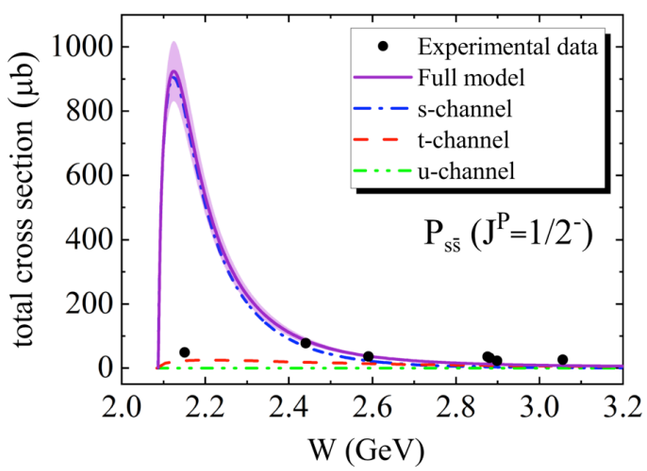

FIG. 8. The total cross section for the reaction $\pi^- p \to K^*\Sigma$. The band stands for the error bar of the five fitting parameters in Table II. The solid (purple), dashed-dotted (blue), dashed (red), dash–double dotted (green) lines are for the full model, the s-channel, the t-channel and the u-channel, respectively. Here, the spin-parity quantum number of the $P_{s\bar{s}}$ is $\frac{1}{2}^-$.

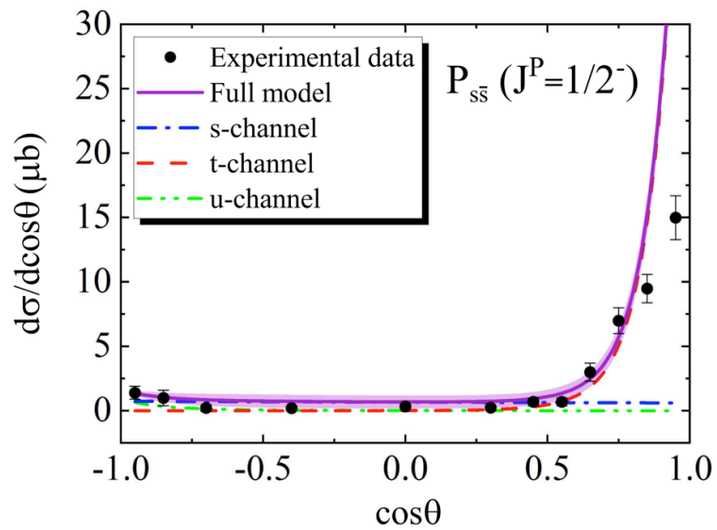

FIG. 9. The differential cross section $d\sigma/d\cos\theta$ for the $\pi^- p \to K^*\Sigma$ reaction as a function of $\cos\theta$. The experimental data are from Ref. [35]. Here, the notation is the same as that in Fig. 8.

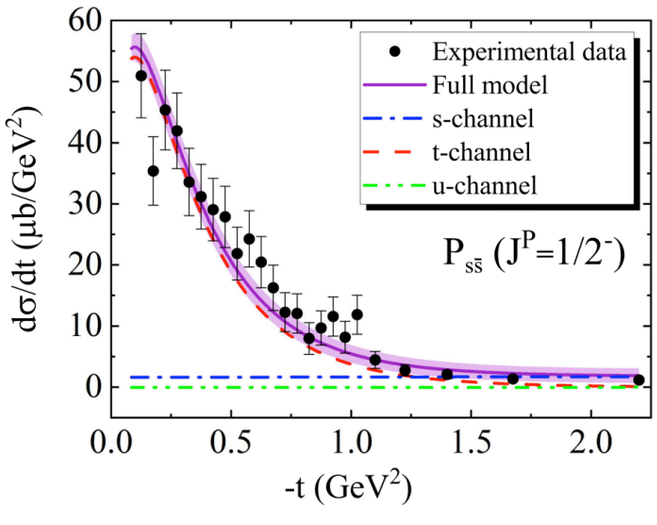

FIG. 10. The t distribution for the reaction $\pi^- p \to K^*\Sigma$. The experimental data are from Ref. [36]. Here, the notation is the same as that in Fig. 8.

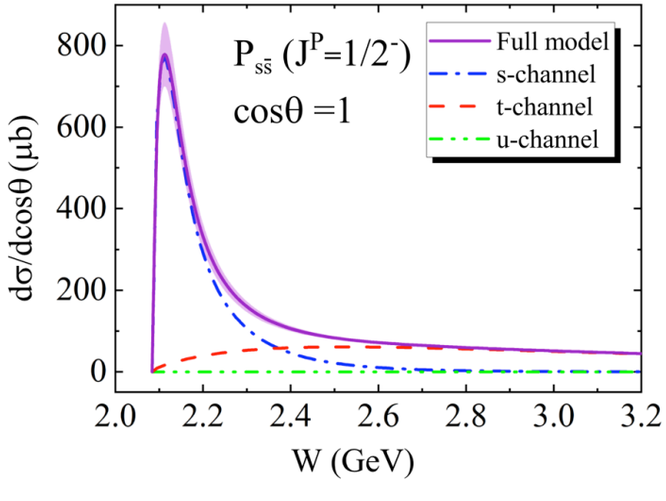

FIG. 11. The differential cross-section $d\sigma/d\cos\theta$ for the $\pi^- p \to K^*\Sigma$ reaction varies with different c.m. energies when $\cos\theta = 1$. Here, the notation is the same as that in Fig. 8.

3. Production of hidden-strange molecular pentaquark

PHYSICAL REVIEW D **110,** 014026 (2024)

Prospects for detecting the hidden-strange pentaquarklike state $N^*(2080)$ in the $\pi^- p \to \phi n$ reaction

Xiao-Yun Wang,[1,2,*] Hui-Fang Zhou,[1] and Xiang Liu[3,2,4,5,6,†]

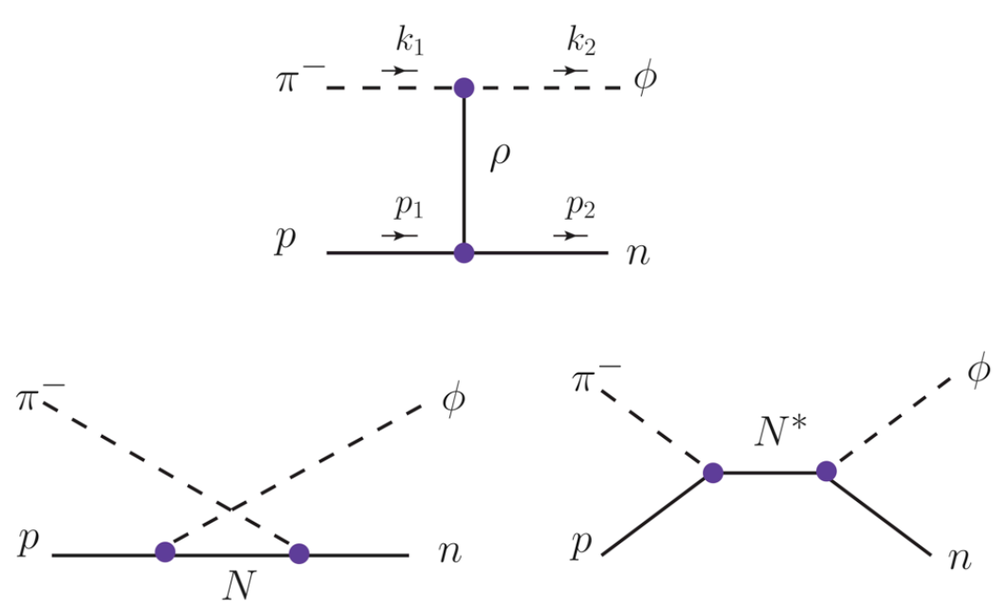

FIG. 1. Feynman diagrams for the $\pi^- p \to \phi n$ reaction. The top figure is the t-channel tree diagram, while the bottom left and bottom right are the tree diagrams of u-channel and s-channel, respectively.

With the above preparation, the amplitude of the $\pi^- p \to \phi n$ reaction can be written as

$$-i\mathcal{M} = \epsilon^{\mu}(k_2)\bar{u}(p_2)(\mathcal{A}_t^{\rho} + \mathcal{A}_u^{N} + \mathcal{A}_s^{N^*})u(\rho_1), \tag{17}$$

where ϵ_μ is the polarization vector of the ϕ meson. $\bar{u}$ or u denotes the Dirac spinor of the nucleon. The reduced amplitudes $\mathcal{A}_t^{\rho}$, $\mathcal{A}_s^{N^*}$ and $\mathcal{A}_u^{N}$ for the t-channel, s-channel, and u-channel contributions read as

$$\mathcal{A}_t^{\rho} = -\sqrt{2}\frac{g_{\pi\rho\phi}}{m_\phi} g_{\rho NN} F_t(q_t^2) \frac{\mathcal{P}^{\nu\xi}}{t - m_\rho^2} \epsilon_{\mu\nu\alpha\beta} k_2^{\alpha} \times (k_2 - k_1)^{\beta} \left[\gamma_\xi + \frac{\kappa_{\rho NN}}{4m_N}(\gamma_\xi \not{q}_t - \not{q}_t \gamma_\xi)\right], \tag{18}$$

$$\mathcal{A}_u^{N} = -i\sqrt{2} g_{\pi NN} g_{\phi NN} F_u(q_N) \left[\gamma_\mu + \frac{\kappa_{\phi NN}}{4m_N}(\gamma_\mu \not{k}_2 - \not{k}_2 \gamma_\mu)\right] \times \frac{(\not{q}_N + m_N)}{u - m_N^2}\gamma_5, \tag{19}$$

$$\mathcal{A}_s^{N^*(3/2^-)} = \sqrt{2}\frac{g_{\pi NN^*}^{3/2^-}}{m_\pi} \frac{-ig_{N^*\phi N}^{3/2^-}}{2m_N} F_s(q_s^2)\gamma^{\sigma}(k_{2\beta} g_{\mu\sigma} - k_{2\sigma} g_{\mu\beta}) \frac{(\not{q}_s + m_{N^*})}{s - m_{N^*}^2 + i m_{N^*}\Gamma_{N^*}} \Delta^{\beta\alpha} k_{1\alpha}\gamma_5, \tag{20}$$

$$\mathcal{A}_s^{N^*(1/2^-)} = \sqrt{2} g_{\pi NN^*}^{1/2^-} g_{N^*\phi N}^{1/2^-} F_s(q_s^2)\gamma_5\gamma_\mu \frac{(\not{q}_s + m_{N^*})}{s - m_{N^*}^2 + i m_{N^*}\Gamma_{N^*}}, \tag{21}$$

3. Production of hidden-strange molecular pentaquark

$$J^P = 3/2^+ : P_{s\bar{s}}[3/2^-]$$

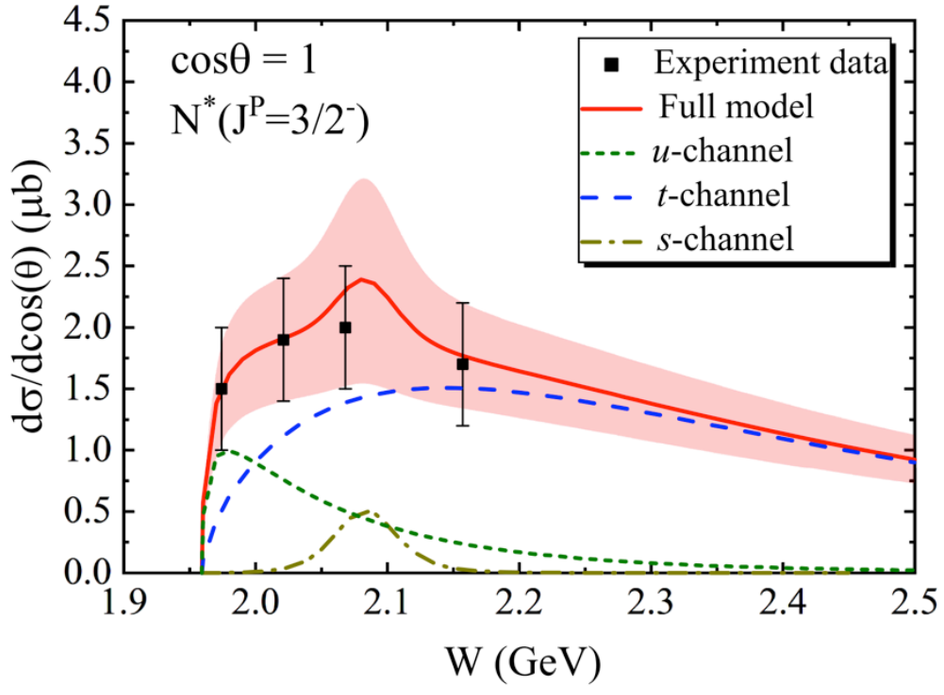

FIG. 2. The differential cross section of the $\pi^- p \to \phi n$ reaction varies with different c.m. energies when $\cos\theta = 1$. The experimental data are taken from Ref. [77]. The band stands for the error bar of the three fitting parameters in Table I. The solid (red), short-dashed (green), dashed (blue), and dashed-dotted (dark yellow) lines are for the full model, the u-channel, the t-channel and the s-channel, respectively. Here, the spin-parity quantum number of the $N^*(2080)$ is $\frac{3}{2}^-$.

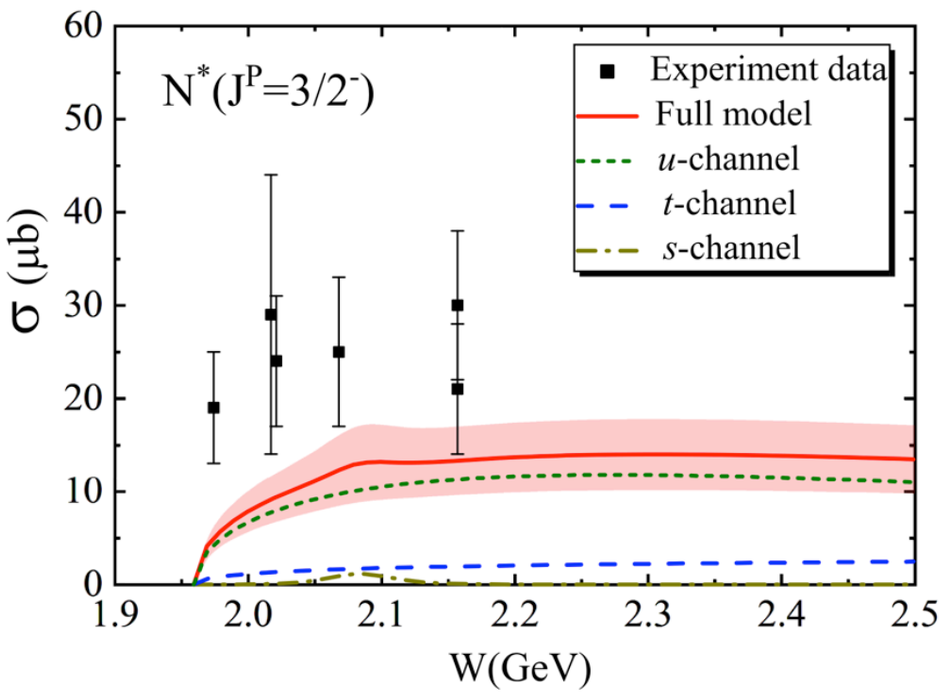

FIG. 3. The total cross section for the reaction of $\pi^- p \to \phi n$. The experimental data are taken from Refs. [77,78]. The band stands for the error bar of the three fitting parameters in Table I. Here, the notation is the same as that in Fig. 2.

3. Production of hidden-strange molecular pentaquark

$$J^P = 1/2^+ : P_{s\bar{s}}[1/2^-]$$

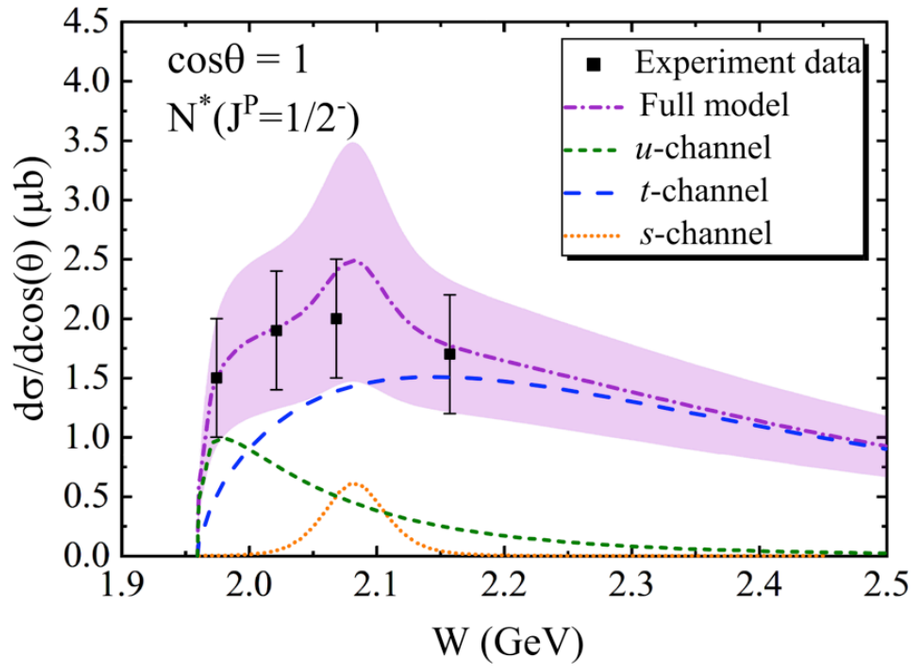

FIG. 6. The differential cross section of the $\pi^- p \to \phi n$ reaction varies with different c.m. energies when $\cos\theta = 1$. The experimental data are taken from Ref. [77]. The band stands for the error bar of the three fitting parameters in Table II. The short-dashed dotted (purple), short-dashed (green), dashed (blue), and short-dotted (orange) lines are for the full model, the u-channel, the t-channel, and the s-channel, respectively. Here, the spin-parity quantum number of the $N^*(2080)$ is $\frac{1}{2}^-$.

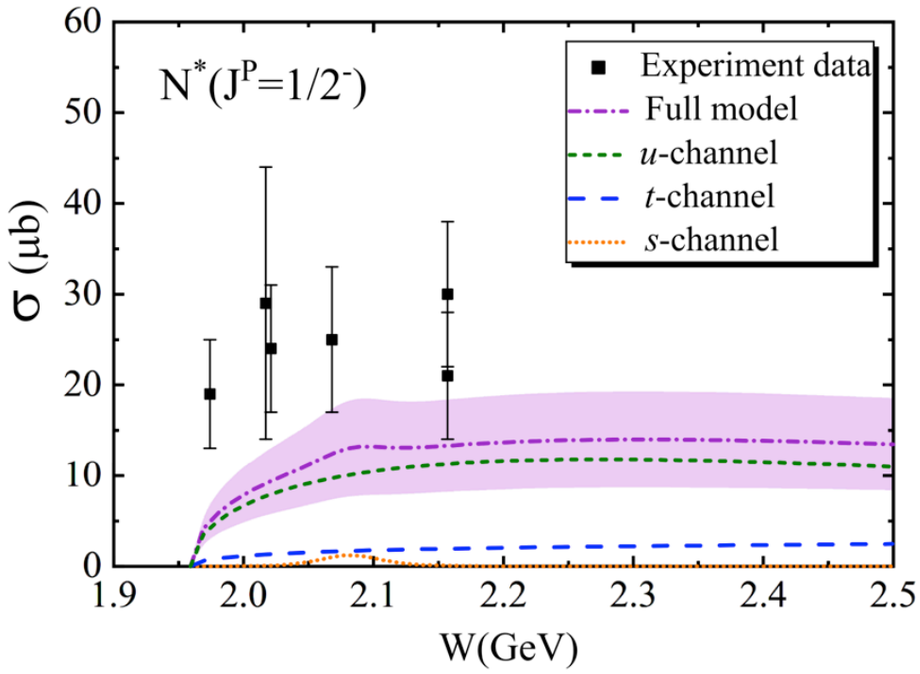

FIG. 7. The total cross section for the reaction of $\pi^- p \to \phi n$ The experimental data are taken from Ref. [77,78]. The banc stands for the error bar of the three fitting parameters in Table II The notation is the same as in Fig. 6.

4. Production of high-spin ω_J and ρ_J $(J = 2,3,4,5)$

PHYSICAL REVIEW D **113,** 054050 (2026)

Production of high-spin ω_J and ρ_J $(J = 2, 3, 4, 5)$ mesons in $\pi^- p$ reactions

Ting-Yan Li,* Zi-Yue Bai,† and Xiang Liu‡

School of Physical Science and Technology, Lanzhou University, Lanzhou 730000, China;
Lanzhou Center for Theoretical Physics, Key Laboratory of Theoretical Physics of Gansu Province, Key Laboratory of Quantum Theory and Applications of MoE, Gansu Provincial Research Center for Basic Disciplines of Quantum Physics, Lanzhou University, Lanzhou 730000, China;
MoE Frontiers Science Center for Rare Isotopes, Lanzhou University, Lanzhou 730000, China;
and Research Center for Hadron and CSR Physics, Lanzhou University
and Institute of Modern Physics of CAS, Lanzhou 730000, China

(Received 28 January 2026; accepted 10 March 2026; published 30 March 2026)

In this work, we perform a comprehensive investigation of the production of high-spin ω_J and ρ_J mesons $(J = 2, 3, 4, 5)$ in $\pi^- p$ reactions using an effective Lagrangian approach. By constructing the relevant t-channel processes and calibrating the model with a single adjustable parameter fitted to existing data, we successfully reproduce the measured total and differential cross sections for the $J = 3$ states $\omega_3(1670)$ and $\rho_3(1690)$. Within the same framework, we predict the production cross sections for their lower- and higher-spin partners; $\omega_2(1975)$, $\rho_2(1940)$, $\omega_4(2250)$, $\rho_4(2230)$, $\omega_5(2350)$, and $\rho_5(2350)$. Our results show that these states exhibit measurable cross sections with characteristically forward-peaked angular distributions, underscoring their strong potential for observation in future πp meson-beam experiments.

4. Production of high-spin ω_J and ρ_J $(J = 2,3,4,5)$

PHYSICAL REVIEW D **113,** 054050 (2026)

Production of high-spin ω_J and ρ_J $(J=2, 3, 4, 5)$ mesons in $\pi^- p$ reactions

Ting-Yan Li,* Zi-Yue Bai,† and Xiang Liu‡

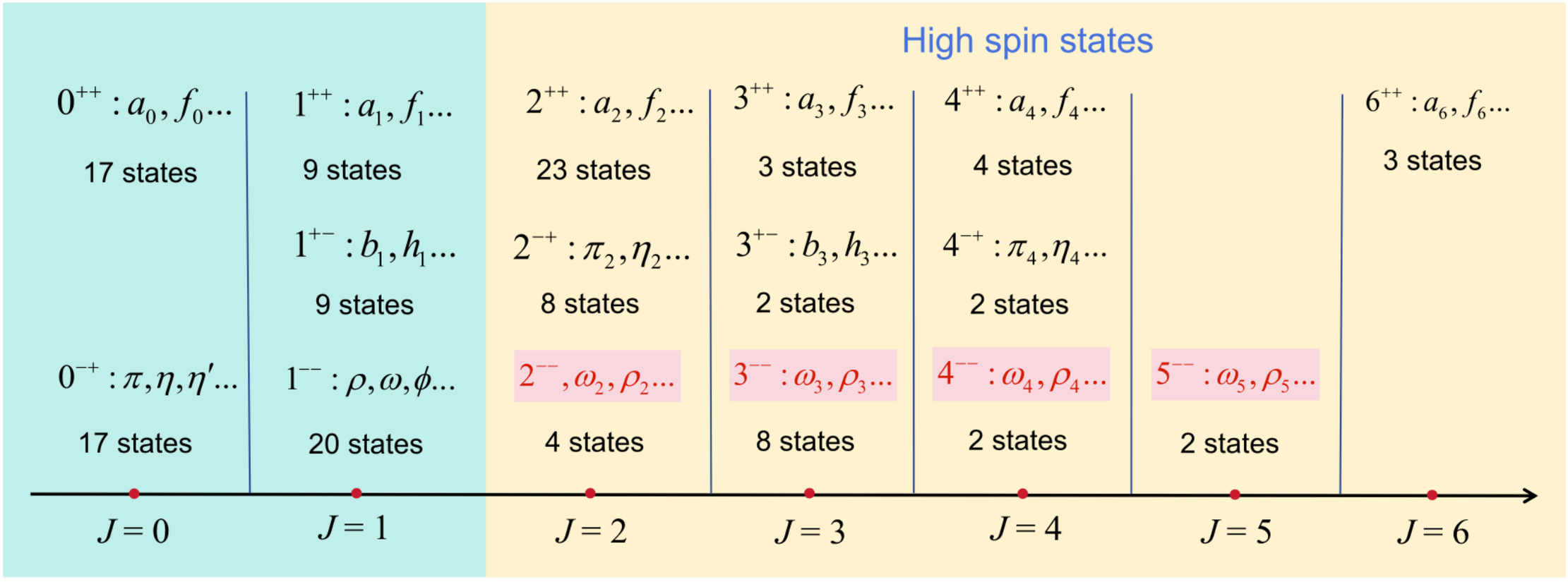

FIG. 1. A concise summary of light mesons [1].

4. Production of high-spin ω_J and ρ_J $(J = 2,3,4,5)$

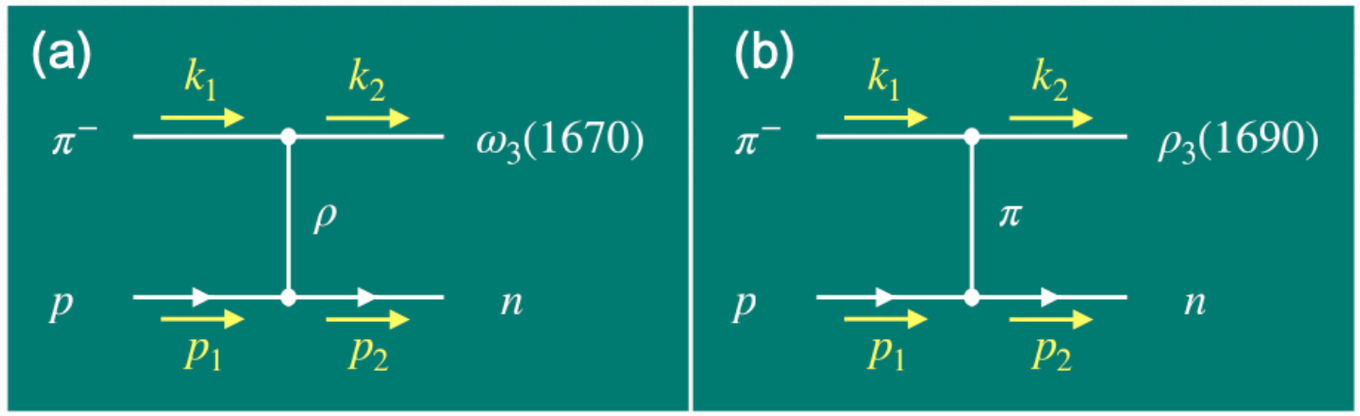

FIG. 2. Feynman diagrams for the $\pi^- p \to \omega_3(1670)n$ (a) and $\pi^- p \to \rho_3(1690)n$ (b) reactions.

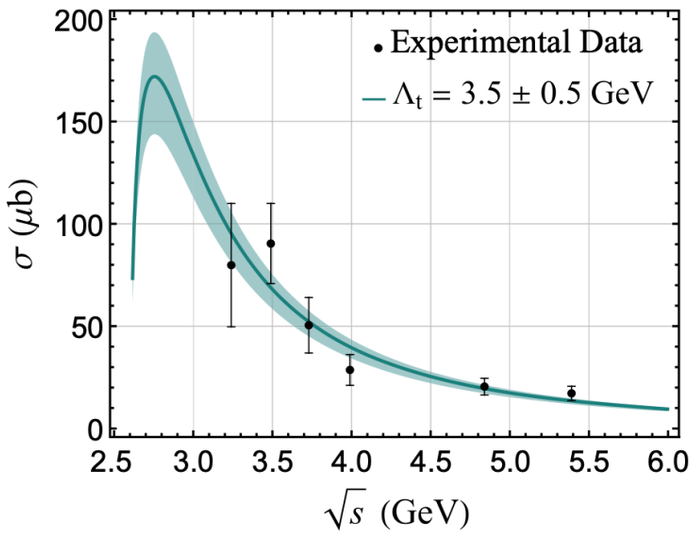

FIG. 3. The total cross section for the reaction $\pi^- p \to \omega_3(1670)n$. The black points with error bars correspond to the experimental data from Refs. [16,17,21–23].

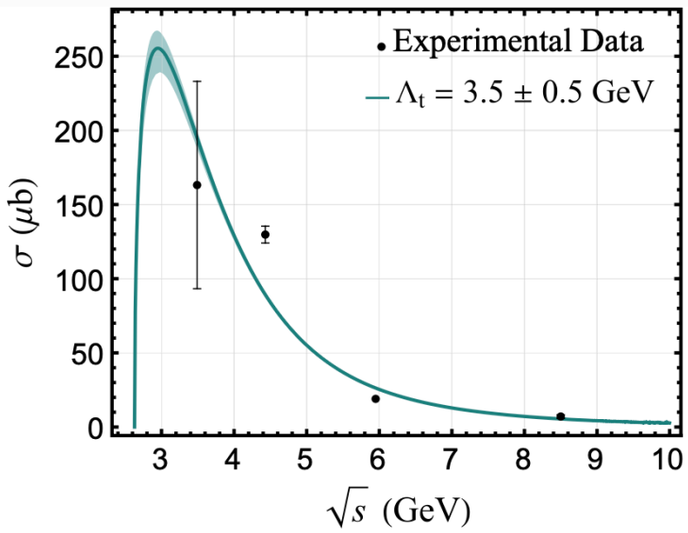

FIG. 5. The total cross section for the reaction $\pi^- p \to \rho_3(1690)n$. The black points with error bars correspond to the experimental data from Refs. [18,24–26].

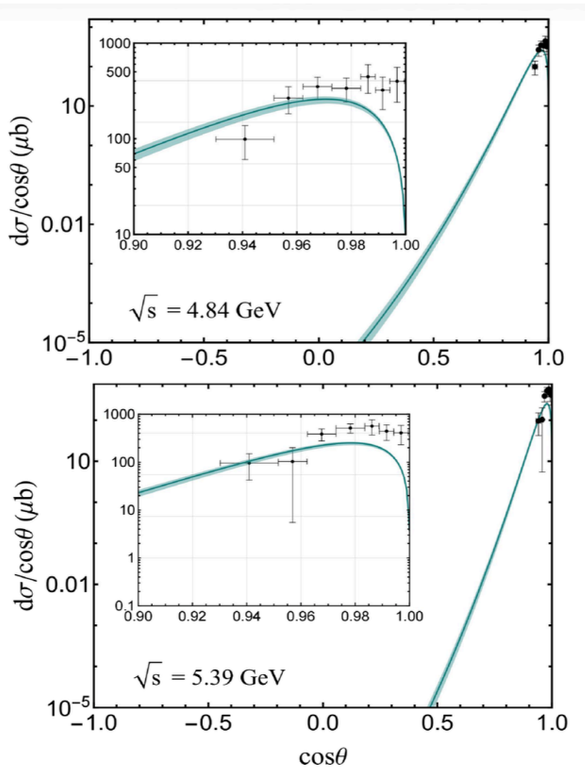

FIG. 4. The differential cross section $d\sigma/d\cos\theta$ of the $\omega_3(1670)$ production at different c.m. energy E_{cm}. The black points with error bars correspond to the experimental data from Ref. [17].

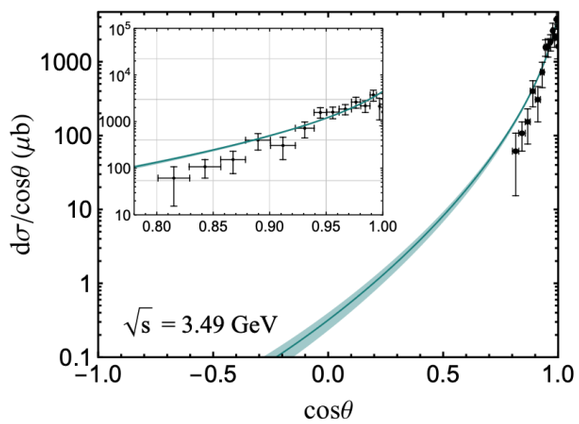

FIG. 6. The differential cross section $d\sigma/d\cos\theta$ of the $\rho_3(1690)$ production at c.m. energy $E_{cm} = 3.49$ GeV. The black points with error bars correspond to the experimental data from Ref. [18].

4. Production of high-spin ω_J and ρ_J $(J = 2,3,4,5)$

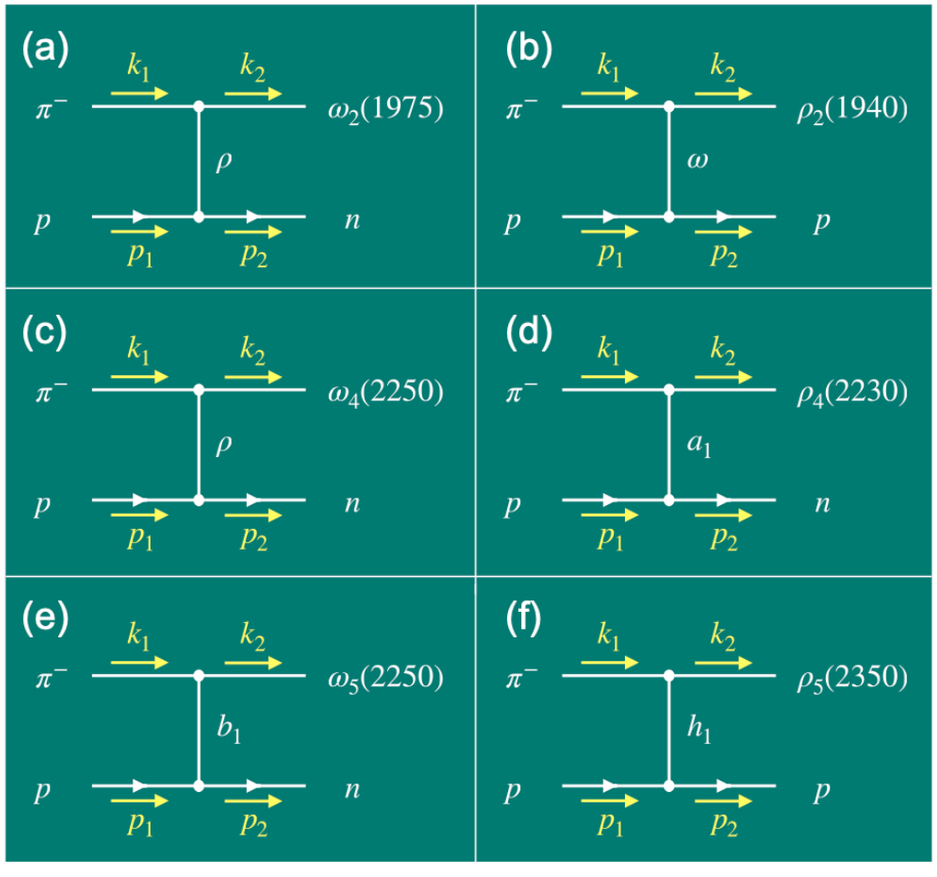

FIG. 7. Feynman diagrams for the $\pi^- p \to \omega_J/\rho_J + N$ reactions.

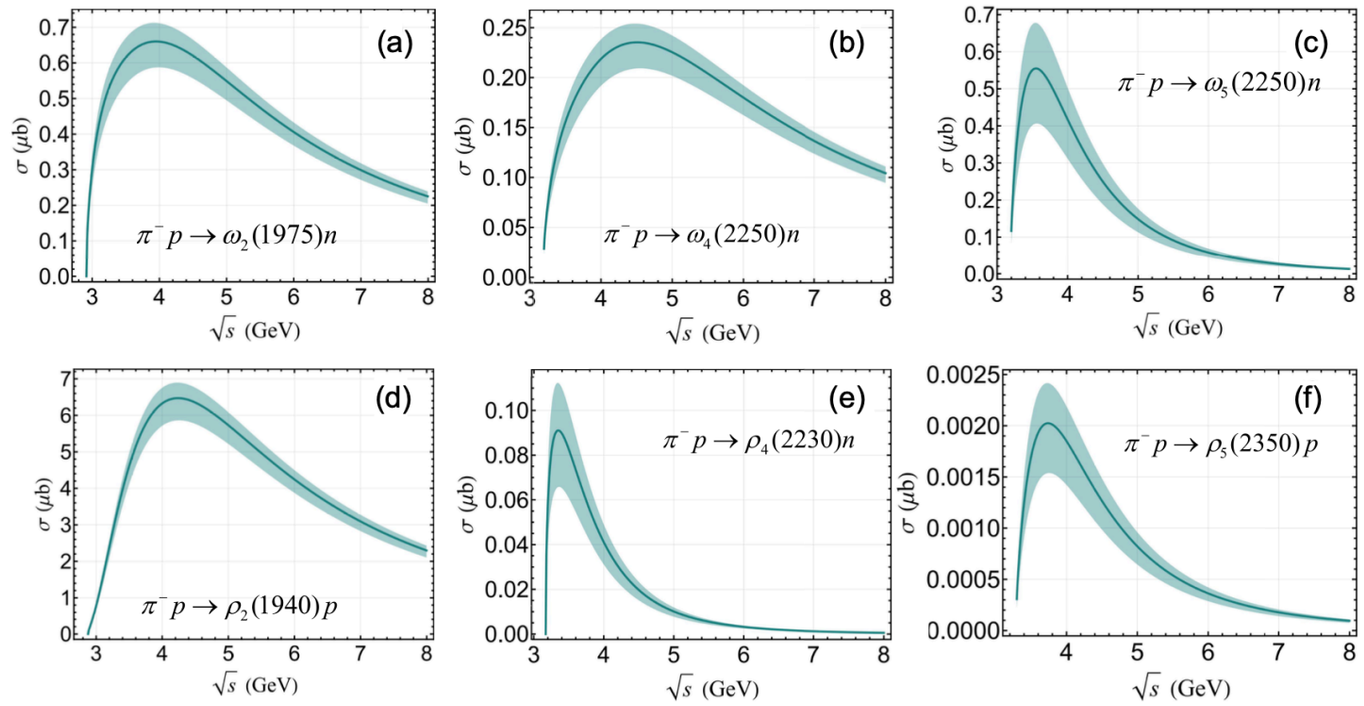

FIG. 8. The energy dependence of the total cross section for production of the $\omega_2(1975)$, $\rho_2(1940)$, $\omega_4(2250)$, $\rho_4(2230)$, $\omega_5(2250)$, $\rho_5(2350)$ through t-channel with cutoff $\Lambda_t = 3.5 \pm 0.5$ GeV.

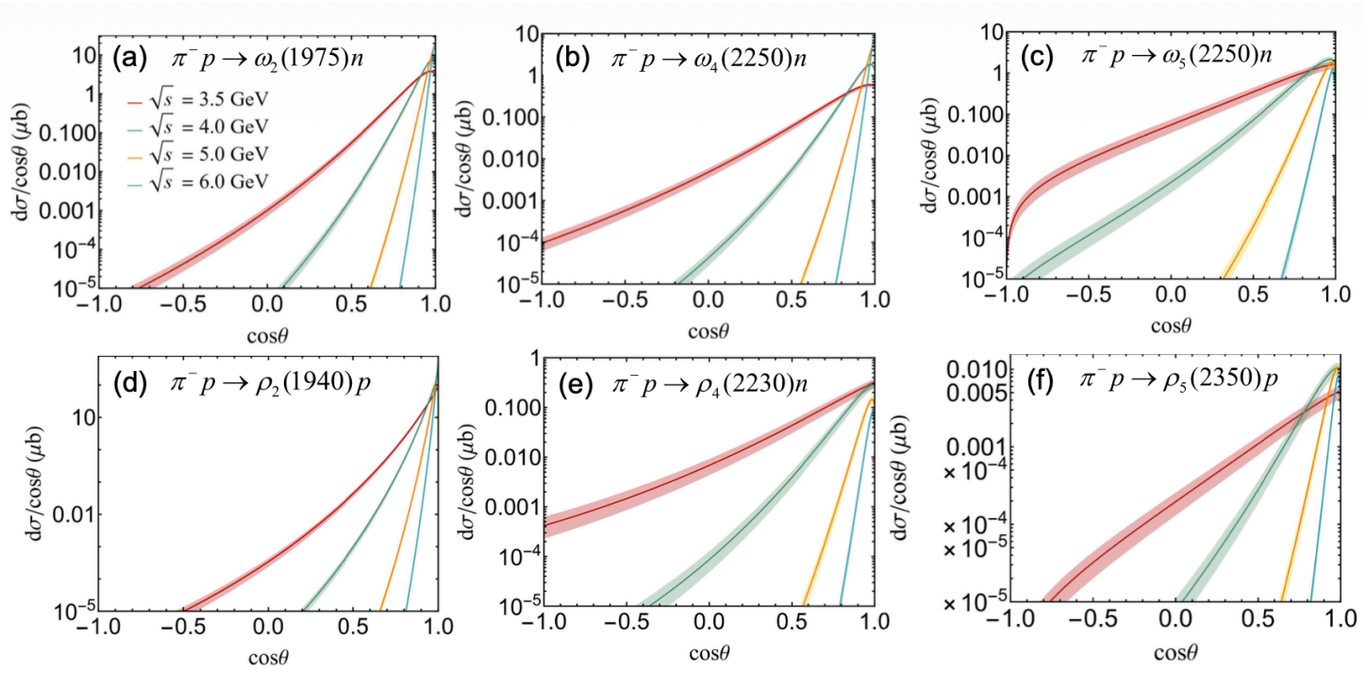

FIG. 9. The differential cross section $d\sigma/d\cos\theta$ of the $\omega_2(1975)$, $\rho_2(1940)$, $\omega_4(2250)$, $\rho_4(2230)$, $\omega_5(2250)$, $\rho_5(2350)$ production at different c.m. energies W = 3.5, 4, 5 and 6 GeV.

5. Summary

Opportunity for HIAF for building meson bean experiment

图 8　(在线彩图) HIAF 总体布局图[102]

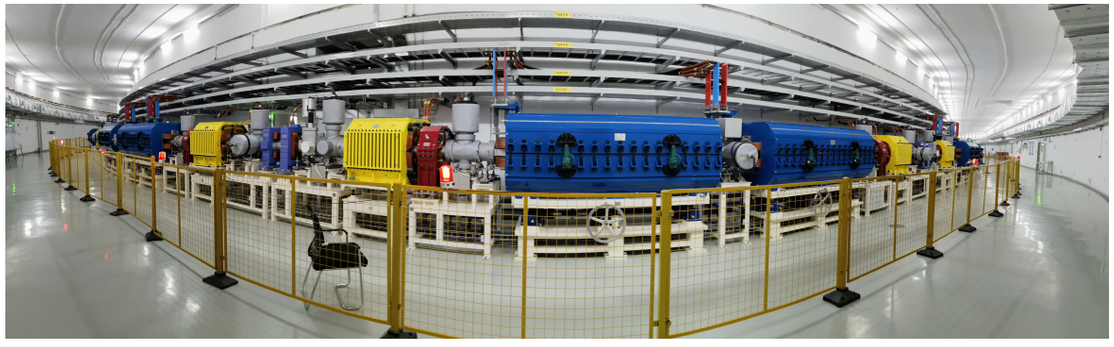

5. Summary

Opportunity for HIAF for building meson bean experiment

表 9　基于 HIAF 的质子束流可能产生的次级介子束流参数

介子束流能量/GeV	动量分散	束流强度(以每脉冲的粒子数为单位)
4	±3%	束流强度预计比主质子束流低100倍，约为 2.0×10^{10}
6	±3%	束流强度预计比主质子束流低1 000倍，约为 2.0×10^{9}
8	±3%	束流强度预计比主质子束流低4个量级，约为 2.0×10^{8}

表 10　未来 HIAF 上的介子束流实验可以测量的部分散射过程

$\pi^-p\rightarrow f_1(1285)n$	$K^-p\rightarrow f_1(1285)\Lambda$	$\pi^-p\rightarrow f_1(1420)n$	$K^-p\rightarrow f_1(1420)\Lambda$
$K^-p\rightarrow a_0(1817)\Lambda$	$K^-p\rightarrow \eta_1(1855)\Lambda$	$K^-p\rightarrow \phi(2170)\Lambda$	$K^-p\rightarrow \eta(2225)\Lambda$
$K^-p\rightarrow K^{(*)}N^{(*)}$	$\pi^-p\rightarrow K^{(*)}\Sigma^{(*)}$	$\pi^-p\rightarrow K^{(*)}\Lambda^{(*)}$	$\pi^-p\rightarrow K^{(*)}\Lambda(1405)$
$\pi^-p\rightarrow K^{(*)}\Lambda(1520)$	$K^-p\rightarrow K^{(*)}\Xi^{(*)}$	$\pi^-p\rightarrow \phi n$	$K^-p\rightarrow \phi\Sigma^{(*)}$
$K^-p\rightarrow \phi\Lambda$	$K^-p\rightarrow \phi(1850)\Lambda$	$K^-p\rightarrow \phi\Lambda(1405)$	$K^-p\rightarrow \phi\Lambda(1520)$

But not limited to these

Thank you for your attention!